Preparation of thiol modified Fe_3O_4@Ag magnetic SERS probe for PAHs detection and identification

Jingjing Du, Chuanyong Jing*

State Key Laboratory of Environmental Chemistry and Ecotoxicology,
Research Center for Eco-Environmental Sciences,
Chinese Academy of Sciences, Beijing 100085, China

Tel: +86 10 6284 9523; Fax: +86 10 6284 9523

E-mail: cyjing@rcees.ac.cn

Abstract

In situ detection and identification of PAHs, a group of well-known persistent organic pollutants, presents a great challenge to environmental researchers. This study developed a novel substrate based on thiol-functionalized Fe_3O_4@Ag core-shell magnetic nanoparticles for surface enhanced Raman scattering (SERS) sensing of PAHs. The surface morphology, structure, and magnetic properties of the substrate were characterized using multiple complimentary techniques including transmission electron microscopy, energy-dispersive X-ray spectroscopy, vibrating sample magnetometry analysis, and extended X-ray absorption fine structure spectroscopy. The high saturation magnetization at 48.35 emu g^{-1} enabled the complete and rapid separation of the substrate from the PAHs solution. Benzene, naphthalene, anthracene, phenanthrene, fluorene, pyrene, perylene, and BaP were chosen as probe molecules. Qualitative and quantitative determination of PAHs was achieved using a portable Raman spectrometer. The SERS sensitivity was positively correlated with the hydrophobic nature of PAHs. The SERS response exhibited a linear dependence on the PAHs concentration between 1 to 50 mg/L, and the detection limit in the order 10^{-5} to 10^{-7} M was obtained. The SERS platform with magnetic substrate provides a new way for *in situ* PAHs monitoring.

Keywords: SERS; PAHs; magnetic; core-shell; modification

Introduction

Polycyclic aromatic hydrocarbons (PAHs) are mainly formed during the incomplete combustion of coal and fuels.[1] Most PAHs are highly carcinogenic and persistent in the environment and their concentrations could accumulate up to 300 g/kg in some coal gasification sites.[2,3] According to a recent review, the total PAHs in nature water sources may reach the mg/L level despite their hydrophobic properties.[4] Traditional PAHs identification and quantification methods heavily rely on the usage of expensive instrumentation including high performance liquid chromatography (HPLC), gas chromatography (GC), and GC/mass spectrometry (MS). Most conventional analysis techniques also need a pre-concentration step, which is time and labor-consuming.[5]

In general, PAHs are not present individually but in mixtures, which makes the *in situ* identification of PAHs a challenge.[6] Recently, the surface-enhanced Raman scattering (SERS) provides an alternative method for environmental analyses mainly due to its substantial electromagnetic enhancement induced by local surface plasmon resonance.[7,8] SERS-active analytes must generally have an inherent affinity towards the noble metal surface, where the electromagnetic fields are localized. Unfortunately, the apolar nature of PAHs prevents their approach to polar metal surfaces, thus limiting the SERS application in PAHs detection. Therefore, two approaches have been investigated: the first one is functionalizing silver colloids to capture PAHs to metal surfaces. The

functional entities include calixarenes,[9] dicarbamates,[10] viologen,[11] humic acids,[12] and cyclodextrin.[13] Another method is employing self-assembled thiol and alkylsilane monolayers on the immobilized SERS substrate,[14-17] which makes the metal surface hydrophobic and consequently capable of PAHs adsorption.

SERS substrates are commonly colloidal or immobilized noble metal nanopartilces (NPs). The passive contact between these NPs and the target analyte may constrain the active concentrating of the analyte to the substrate. During the last decades, functionalized core–shell magnetic NPs have been widely investigated with respect to industrial, biomedical, and environmental applications.[18-20] Many efforts have been made to fabricate uniform nanostructures such as silica-coated, silver-coated, and gold-coated magnetic NPs.[21-23] Our recent study shows that with the introduction of functionalized core–shell magnetic NPs, environmental pollutants could be actively adsorbed to the vicinity of SERS substrate and subsequently the SERS sensitivity could be enhanced.[24]

The purpose of this study is to provide a potential application platform for monitoring of PAHs contamination. In the present report, we synthesized a sensitive and recyclable SERS substrate for PAHs identification and detection based on thiol-functionalized Fe_3O_4@Ag core-shell magnetic nanomaterial. Benzene and seven PAHs were selected because of their different size and structure, ranging from one to five aromatic-rings (Figure 1), and acridine was chosen as a control. Because thiol layer could embed the

77 analyte onto the substrate surface, qualitative and quantitative determination of PAHs
78 with good selectivity was achieved using a portable Raman spectrometer. To the best of
79 our knowledge, it is the first time functionalized core-shell magnetic NPs have been used
80 in PAHs determination.

81 **Experimental Methods**

82 **Reagents.** All reagents were of analytical reagent grade and used without further
83 purification. Ferric chloride and ferrous chloride were obtained from Beijing Chemicals
84 Corporation (China); silver nitrate (>99.8%), aqueous ammonia (25%), sodium
85 hydroxide (>99.5%), absolute ethanol and hydroxylamine hydrochloride (>99.5%) were
86 from Beijing Chemical Reagents Company (China). PAHs were purchased from J&K
87 Scientific Ltd. (China), 3-aminopropyltrimethoxysilane (APTMS, 97%) was from
88 Aldrich Chemicals Corporation (USA). 1-pentanethiol (99%) was purchased from Tokyo
89 Chemical Industry. Co. Ltd. (Japan), and was referred to as C5 for brevity. Milli-Q water
90 was used in all experiments. A standard reference material, the coal fly ash sample (GBW
91 08403) were obtained from the State Quality Inspection Administration of China, and
92 their concentrations are listed in Table S1 in the Supporting Information (SI).

93 **Preparation of thoil functionalized Fe_3O_4@Ag NPs.** The protocol used for substrate
94 preparation and SERS detection of PAHs is shown in Figure 2. The magnetic Fe_3O_4@Ag
95 NPs were prepared following our previous work.[24] The as-prepared Fe_3O_4@Ag particles

were washed by ethanol three times and redispersed in 10 mL ethanol. To the above solutions, 10 μL thiol was slowly added and the reaction was kept for 4 h. The product was washed with 20 mL ethanol twice to remove the excess thiol. The thiol coated substrate can be stored in ethanol for more than three months before use.

Characterization. The size and morphology of Fe_3O_4 and Fe_3O_4@Ag NPs were characterized by transmission electron microscopy (TEM, JEM-1400 from JEOL Ltd.) The energy dispersive X-ray spectrometry (EDX) analysis was carried out using a HITACHI S-3000N SEM with an Oxford energy dispersive X-ray analyzer. Magnetic properties were measured by a vibration sample magnetometer at room temperature. Raman and SERS spectra were obtained using a portable Raman spectrometer (Enwave Optronics, Inc. USA) with a 4 cm^{-1} resolution at 785 nm excitation energy. The EXAFS spectra at the Ag K-edge (25,514 eV) were collected at beamline BL01C at National Synchrotron Radiation Research Center, Taiwan. The electron storage ring was operated at 1.5 GeV with a fixed current of 300 mA. The SERS substrate samples were sealed in two layers of Kapton tape and positioned at 45^o to the X-ray beam in a cryostat for fluorescence measurement. The EXAFS data analysis followed the standard procedure detailed in our previous report.[25]

Sample preparation for SERS analysis. The PAHs alcohol solutions were prepared in concentration range 0.1 to 50 mg/L. To collect the SERS spectra of PAHs mixture,

perylene, benzo[a]pyrene (BaP), pyrene, anthracene, and phenanthrene were diluted in ethanol at concentrations of 1.0 and 10 mg/L, respectively. A control sample was also prepared by adding acridine into the PAHs mixture. The thiol-coated NPs were immersed in a 10 mL ethanol solution containing various concentrations of PAHs for 1 h. Then, the NPs were assembled by an applied magnetic field, and exposed to the laser for 5 s to measure the SERS signal.

Result and Discussion

Substrate characterization. The TEM micrograph in Figure 3 demonstrates that Fe_3O_4@Ag NPs with particle size of 50 ± 20 nm and silver shell thickness at 5 nm were successfully synthesized. The EDX spectrum as shown in SI Figure S1 also served as an important evidence for the existence of Ag shell on the Fe_3O_4 surface. The superpara magnetism of Fe_3O_4@Ag NPs was confirmed with a vibrating sample magnetometer. The maximum magnetic strength was evaluated by the saturation magnetization (SM), which were 59.15 emu/g for Fe_3O_4 and 48.35 emu/g for Fe_3O_4@Ag NPs (Figure S2). The slight decrease in SM due to Ag coating did not hamper the magnetic separation, because a SM value higher than 16.3 emu/g is sufficient to achieve magnetic separation.[26] The k^3-weighted Ag K-edge EXAFS spectra are shown in Figure 4-I, and the corresponding radial structure functions are shown in Figure 4-II as magnitude of the Fourier transformation versus radial distance. The EXAFS results listed in SI Table S2

demonstrate the formation of metallic Ag nanoparticles in the substrate with a first shell distance of 0.287 nm.[27]

Functionalization of substrate with thiol. Functionalization of Fe_3O_4@Ag NPs with 1-pentanethiol (C5) was confirmed with SERS spectra illustrated in Figure 5-I. After coating C5 on Fe_3O_4@Ag NPs, the Raman shifts were observed at 638 cm^{-1} (gauche C-S stretch), 700 cm^{-1} (trans C-S stretch), 744 cm^{-1} (gauche CH_2 rock), 895 cm^{-1} (CH_3 rock), 1056 cm^{-1} (trans C-C), 1107 cm^{-1} (trans C-C), and 1443 cm^{-1} (CH_3 deformation) (Figure 5-I, c).[28] As compared with normal Raman spectrum of C5 (Figure 5-I, b), a dramatic decrease in intensity at 657 cm^{-1} (gauche C-S stretch) and increase of trans C-S stretch (731 cm^{-1}) was detected upon C5 modification, suggesting the bonding of C5 to Ag through S heading group.[29]

To confirm the formation of self assembled thiol monolayer (SAM) on substrate surface, SERS analysis of acridine was performed as a control experiment. The peak intensity of acridine at 402, 743, 1401, and 1559 cm^{-1} on thiol-modified Ag surface (Figure 5-II, c) decreased dramatically comparing with that on blank Ag surface (Figure 5-II, b). The peak assignments for acridine are listed in SI Table S3. Because acridine is vertically adsorbed to Ag surface through nitrogen lone pair electrons,[30,31] the force of interactions between acridine and Ag surface would be significantly reduced upon the addition of thiol. Our hypothesized adsorption mechanisms are sketched in Figure 6. The

153 good agreement between observation and proposed mechanism proved the successful
154 formation of SAM on Ag surface.

155 To justify our hypothesis that the PAHs were bound to SAM rather than the surface of
156 Fe_3O_4@Ag NPs, the SERS signals between Fe_3O_4@Ag and Fe_3O_4@Ag@C5 NPs were
157 compared for a mixture of five PAHs and acridine. No PAHs characteristic peak but
158 acridine was observed on the Fe_3O_4@Ag NPs (Figure 7-b). In contrast, characteristic
159 peaks corresponding to each PAHs were observed on the Fe_3O_4@Ag@C5 NPs as shown
160 in Figure 7-d. The stark contrast demonstrates that the PAHs bind to the thiol layer.

161 **Effect of SAM density on SERS sensitivity.** To examine the SAM density on PAHs
162 detection, SERS sensitivity of anthracene, pyrene, and perylene as a function of C5
163 concentration was compared. As shown in SI Figure S3, the optimal C5 concentration
164 was 0.08 M. The SAM generated with 0.04 and 0.12 M C5 led to a dramatic decrease in
165 SERS intensity. The results demonstrate the importance of desirable SAM density for the
166 successful adsorption of analyte.

167 **SERS detection of PAHs.** SERS spectra of PAHs on thiol modified substrate are
168 illustrated in Figure 8. The spectra were subtracted from the SERS spectrum of C5 to
169 provide clear information. Figure 8-I shows the SERS difference spectra of perylene, BaP,
170 and pyrene. Normal Raman spectra of the solid PAHs are also presented for comparison,
171 and the positions and assignments of Raman shifts for perylene, BaP, and pyrene are

summarized in SI Tables S4-S6. The SERS peak position of perylene centered at 1571, 1373, 1296, 980, 546, and 362 cm^{-1} corresponded to the Raman shifts of solid perylene.[32] SERS measurement of BaP resulted in peaks at 1583, 1412, 1385, and 1240 cm^{-1}, which is consistent with BaP Raman peaks.[33] In the case of pyrene, small frequency shifts around 2-4 cm^{-1} were observed as compared to its normal Raman spectrum.[34] An intensification was identified with the symmetric a_g mode at 594 cm^{-1} for pyrene, suggesting an enhancement through the Frank-Condon resonance mechanism.[35]

Having detected the three PAHs with 4-5 aromatic rings, SERS measurement of PAHs with three rings was conducted, and the results are shown in Figure 8-II and SI Tables S7-S8. SERS spectrum of anthracene exhibited four major peaks at 393, 756, 1403, and 1555 cm^{-1}.[13,14] Compared with anthracene, phenanthrene with an asymmetrical structure resulted in more SERS peaks at 411, 547, 712, 1044, 1246, 1420, 1441, 1524, and 1570 cm^{-1}.[36] The stability of the substrate after mixing with pyrene was examined by EXAFS analysis as shown in Figure 4. The results suggest that the oxidation state and the local coordination environment of metallic Ag were not changed upon the reaction with PAHs (Table S2).

Chemical selectivity of substrate. In addition to increasing the surface affinity towards PAHs, the functionalization by thiol group enhanced the selectivity of substrate. The lowest detectable concentrations and the octanol-water partition coefficient, K_{ow}, of

each PAHs are shown in Table 1. A decrease of SERS sensitivity was observed following the K_{ow} order perylene > BaP > pyrene > anthracene > phenanthrene. On the other hand, no feature peak was detected for benzene, naphthalene, and fluorene (Figure 8-III). The undetected PAHs have lower molecular mass and K_{ow} than the detectable ones. The substrate preference for larger PAHs may attribute to increased van der Waals interaction, hydrophobicity, and symmetry.

Quantitative analysis of PAHs. To realize the quantitative measurement of PAHs using our technique, SERS spectrum was obtained by exposing the substrate to increasing concentrations of PAHs. The spectra were averaged from ten randomly chosen points on one substrate to obtain reliable results. Since the concentration of C5 was kept constant, the most pronounced C5 band at 895 cm^{-1} was chosen as a reference peak for the spectra normalization. The intensity ratio of the PAHs bands listed in Table 1 to the C5 bands at 895 cm^{-1} was employed to study the SERS sensitivity as a function of PAHs concentrations. As shown in Figure 9, the SERS signal was linearly correlated with the PAHs concentration with a R^2 range 0.937 to 0.987. A linear response between PAH concentration and SERS peak magnitude was also observed by Carron et al..[37] The enhancement factor (EF) for each PAHs was calculated using an equation reported in a previous study.[38] As shown in Table 1, the EF in the order of 10^3 to 10^5 was achieved for small and large PAHs, respectively.

Identification of PAHs. Having successfully detected the five PAHs, the thiol functionalized magnetic NPs were also applied in SERS sensing of PAHs in more complex mixtures. The obtained spectra are shown in Figure 10. The key SERS peaks of individual PAHs also are clearly observed and distinguished in the more complex mixture at 1 and 10 mg/L concentration. Furthermore, concentrations of each PAHs in the mixture were calculated using the linear regression equation obtained from Figure 9. Despite the competition among each PAHs, the calculated concentrations (1.03, 1.05, 1.29, and 1.54 mg/L for anthracene, pyrene, perylene, and BaP) were comparable with the added concentration of 1 mg/L. SERS detection of PAHs from the coal fly ash sample was conducted to prove the suitability of our method for screening purposes. A sufficient number of characteristic peaks of individual PAHs were clearly resolved (Figure 10-c). These peaks could be used for rapid screening of PAHs. However, the overlap of peak positions at around 390 cm^{-1} prevented the accurate quantitative determination of each PAHs.

Conclusions

The present work has demonstrated a facile method to prepare the SAM-functionalized Fe_3O_4@Ag magnetic SERS substrate. The C5 adsorption modifies the substrate surface for selective PAHs partitioning. The SERS enhancement is observed for the PAHs containing more than three aromatic rings. Qualitative and quantitative determination of

PAHs with detection limit at μg/L level was achieved, and the SERS response exhibited a linear dependence on PAHs concentrations between 1 to 50 mg/L. The present approach does not require expensive instrumentation or large sample volumes, which should have great applications in the rapid identification of PAHs in complex samples. The sensitivity of this analytical method have opened a new way towards a generalized use of our technique, not only in the laboratory but also in field assays with a portable Raman spectrometer.

Acknowledgements. We acknowledge Dr. Ting-Shan Chan on beamline BL01C1 at the National Synchrotron Radiation Research Center (NSRRC) for the assistance with XAS data collection. The research is support by the National Natural Science Foundation of China (20890112, 20921703), the National Hi-tech Research Program of China (2009AA061603), and the National Basic Research Program of China (2009CB421601).

Supporting Information Available: EDX spectra of Fe_3O_4@Ag magnetic nanoparticles; The hysteresis loop of Fe_3O_4 and Fe_3O_4@Ag magnetic nanoparticles; The peak intensity of PAHs as a function of C5 concentration; The pretreatment procedure and PAHs concentrations in the coal fly ash sample; Ag K-edge EXAFS fitting results of Fe_3O_4@Ag and Fe_3O_4@Ag@C5 reacted with PAHs; Experimental Raman frequencies of acridine, perylene, BaP, pyrene, anthracene, and phenanthrene.

References

(1) Alvarez-Puebla, R. A.; Dos Santos, D. S.; Aroca, R. F. *Analyst* **2007**, *132*, 1210-1214.

(2) Plaza-Bolanos, P.; Frenich, A. G.; Vidal, J. L. M. *J. Chromatogr. A* **2010**, *1217*, 6303-6326.

(3) Loick, N.; Hobbs, P. J.; Hale, M. D. C.; Jones, D. L. *Crit. Rev. Environ. Sci. Technol.* **2009**, *39*, 271-332.

(4) Srogi, K. *Environ. Chem. Lett.* **2007**, *5*, 169-195.

(5) Schmidt, H.; Ha, N. B.; Pfannkuche, J.; Amann, H.; Kronfeldt, H. D.; Kowalewska, G. *Mar. Pollut. Bull.* **2004**, *49*, 229-234.

(6) Chen, L.; Zhang, Y.; Liu, B. *Talanta* **2010**, *83*, 324-331.

(7) Halvorson, R. A.; Vikesland, P. J. *Environ. Sci. Technol.* **2010**, *44*, 7749-7755.

(8) Schwartzberg, A. M.; Zhang, J. Z. *J. Phys. Chem. C* **2008**, *112*, 10323-10337.

(9) Leyton, P.; Sanchez-Cortes, S.; Campos-Vallette, M.; Domingo, C.; Garcia-Ramos, J. V.; Saitz, C. *Appl. Spectrosc.* **2005**, *59*, 1009-1015.

(10) Guerrini, L.; Garcia-Ramos, J. V.; Domingo, C.; Sanchez-Cortes, S. *Anal. Chem.* **2009**, *81*, 953-960.

(11) Guerrini, L.; Garcia-Ramos, J. V.; Domingo, C.; Sanchez-Cortes, S. *J. Phys. Chem. C* **2008**, *112*, 7527-7530.

(12) Leyton, P.; Cordova, I.; Lizama-Vergara, P. A.; Gomez-Jeria, J. S.; Aliaga, A. E.; Campos-Vallette, M. M.; Clavijo, E.; Garcia-Ramos, J. V.; Sanchez-Cortes, S. *Vib. Spectrosc.* **2008**, *46*, 77-81.

(13) Xie, Y. F.; Wang, X.; Han, X. X.; Xue, X. X.; Ji, W.; Qi, Z. H.; Liu, J. Q.; Zhao, B.; Ozaki, Y. *Analyst* **2010**, *135*, 1389-1394.

(14) Jones, C. L.; Bantz, K. C.; Haynes, C. L. *Anal. Bioanal. Chem.* **2009**, *394*, 303-311.

(15) Costa, J. C. S.; Sant'Ana, A. C.; Corio, P.; Temperini, M. L. A. *Talanta* **2006**, *70*, 1011-1016.

(16) Mosier-Boss, P. A.; Lieberman, S. H. *Anal. Chem.* **2005**, *77*, 1031-1037.

(17) Olson, L. G.; Uibel, R. H.; Harris, J. M. *Appl. Spectrosc.* **2004**, *58*, 1394-1400.

(18) Zhou, X.; Xu, W. L.; Wang, Y.; Kuang, Q.; Shi, Y. F.; Zhong, L. B.; Zhang, Q. Q. *J. Phys. Chem. C* **2010**, *114*, 19607-19613.

(19) Zhao, X.; Shi, Y.; Cai, Y.; Mou, S. *Environ. Sci. Technol.* **2008**, *42*, 1201-1206.

(20) Zhang, X. F.; Clime, L.; Ly, H. Q.; Trudeau, M.; Veres, T. *J. Phys. Chem. C* **2010**, *114*, 18313-18317.

(21) Hu, H. B.; Wang, Z. H.; Pan, L.; Zhao, S. P.; Zhu, S. Y. *J. Phys. Chem. C* **2010**, *114*, 7738-7742.

(22)Mandal, M.; Kundu, S.; Ghosh, S. K.; Panigrahi, S.; Sau, T. K.; Yusuf, S. M.; Pal, T. *J. Colloid Interface Sci.* **2005**, *286*, 187-194.
(23)Xu, Z. C.; Hou, Y. L.; Sun, S. H. *J. Amer. Chem. Soc.* **2007**, *129*, 8698-8699.
(24)Du, J. J.; Jing, C. Y. *J. Colloid Interface Sci.* **2011**, *358*, 54-61.
(25)Pena, M.; Meng, X. G.; Korfiatis, G. P.; Jing, C. Y. *Environ. Sci. Technol.* **2006**, *40*, 1257-1262.
(26)Ma, Z. Y.; Guan, Y. P.; Liu, H. Z. *J. Polym. Sci. Pol. Chem.* **2005**, *43*, 3433-3439.
(27)Harada, M.; Kimura, Y.; Saijo, K.; Ogawa, T.; Isoda, S. *J. Colloid Interface Sci.* **2009**, *339*, 373-381.
(28)Bryant, M. A.; Pemberton, J. E. *J. Amer. Chem. Soc.* **1991**, *113*, 8284-8293.
(29)Bryant, M. A.; Pemberton, J. E. *J. Amer. Chem. Soc.* **1991**, *113*, 3629-3637.
(30)Kaczor, A.; Malek, K.; Baranska, M. *J. Phys. Chem. C* **2010**, *114*, 3909-3917.
(31)Oh, S. T.; Kim, K.; Kim, M. S. *J. Phys. Chem.* **1991**, *95*, 8844-8849.
(32)Shinohara, H.; Yamakita, Y.; Ohno, K. *J. Mol. Struct.* **1998**, *442*, 221-234.
(33)Onchoke, K. K.; Hadad, C. M.; Dutta, P. K. *J. Phys. Chem. A* **2006**, *110*, 76-84.
(34)Sun, B.; Dreger, Z. A.; Gupta, Y. M. *J. Phys. Chem. A* **2008**, *112*, 10546-10551.
(35)Guerrini, L.; Garcia-Ramos, J. V.; Domingo, C.; Sanchez-Cortes, S. *Anal. Chem.* **2009**, *81*, 953-960.
(36)Alajtal, A. I.; Edwards, H. G. M.; Elbagerma, M. A.; Scowen, I. J. *Spectrochimi. Acta, Part A* **2010**, *76*, 1-5.
(37)Carron, K.; Peitersen, L.; Lewis, M. *Environ. Sci. Technol.* **1992**, *26*, 1950-1954.
(38)Le Ru, E. C.; Blackie, E.; Meyer, M.; Etchegoin, P. G. *J. Phys. Chem. C* **2007**, *111*, 13794-13803.
(39)Sverdrup, L. E.; Nielsen, T.; Krogh, P. H. *Environ. Sci. Technol.* **2002**, *36*, 2429-2435.
(40)Sahu, S. K.; Pandit, G. G. *J. Liq. Chromatogr. Relat. Technol.* **2003**, *26*, 135-146.
(41)Xia, G. S.; Ball, W. P. *Environ. Sci. Technol.* **1999**, *33*, 262-269.

318 Table 1. Detection limit of PAHs, K_{ow}, and peak position for

319 quantitative analysis and calculation of enhancement factor.

PAHs	Conc.(mg/L)	Conc.(μM)	EF[a]	Peak (cm^{-1})	log K_{ow}[39-41]
acridine	0.05	0.25	8×10^5	1401	/
perylene	0.2	0.8	1.2×10^5	1571	6.40
BaP	0.2	0.8	8×10^4	1385	6.20
pyrene	1.0	1	1.5×10^4	407	5.20
anthracene	1.0	5	5×10^3	396	4.20
phenanthrene	5.0	20	1.5×10^3	410	4.07
fluorene	/	/	/	/	3.96
naphthalene	/	/	/	/	3.32
benzene	/	/	/	/	2.13

320

321 [a]: Enhance factor, calculated by the following equation: [38]

322 $$EF=(I_{SERS}/I_{RS})(C_{RS}/C_{SERS})$$

323 I_{SERS}: Peak Intensity of the selected Raman band;

324 I_{RS}: The corresponding band intensity of the PAHs neat;

325 C_{RS}/C_{SERS}: The concentration ratio of the PAHs in neat solution and SERS sample.

326

Figure Caption

Figure 1. Molecular structures of analytes in this study.

Figure 2. Schematic representation of the procedure for SERS detection of PAHs.

Figure 3. TEM micrographs of Fe_3O_4 (a) and Fe_3O_4@Ag NPs (b). The HR-TEM image (inset) shows Ag shell thickness of 5 nm.

Figure 4. k^3-weighted observed (dotted line) and model calculated (solid line) Ag K-edge EXAFS spectra (I) and Fourier transform magnitude (II) resulting in a radial distance structure for Fe_3O_4@Ag NPs and pyrene reacted substrate.

Figure 5. (I) Raman spectrum of Fe_3O_4@Ag NPs (a) and C5 (b); SERS spectrum of C5 on Fe_3O_4@Ag NPs (c). (II) Raman spectrum of acridine (a); SERS spectrum of acridine on Fe_3O_4@Ag NPs (b) and C5 modified substrate (c). The concentration of acridine was 1 mg/L.

Figure 6. Schematic representations of adsorption mechanism for acridine.

Figure 7. Raman spectrum of Fe_3O_4@Ag (a); SERS spectrum of C5 on Fe_3O_4@Ag NPs (c); SERS spectrum of PAHs mixture on Fe_3O_4@Ag NPs (b) and Fe_3O_4@Ag@C5 (d). “A” stands for main band of acridine.

Figure 8. (I) Raman spectrum of pyrene (a), BaP (c) and perylene (e); SERS difference spectrum of 1 mg/L pyrene (b), 200 μg/L BaP (d) and 200 μg/L perylene (f). (II) Raman spectrum of phenanthrene (a) and anthracene (c); SERS difference spectrum of 5 mg/L phenanthrene (b), and 1 mg/L anthracene (d). (III) Raman spectrum of benzene (a), naphthalene (c) and fluorene (e); SERS spectrum of 200 mg/L benzene (b), 50 mg/L naphthalene (d) and 50 mg/L fluorene (f).

Figure 9. Calibration curve for perylene (a), BaP (b), pyrene (c), anthracene (d), and phenanthrene (e). The dashed lines show the 95% confidence limits. The data points represented the average ± standard deviation for ten randomly chosen points on substrate. Signal collecting time = 5 s.

Figure 10. Difference SERS spectra of PAHs at the concentration 1 mg/L (a), 10 mg/L (b) and PAHs extracted from the coal fly ash sample (c).

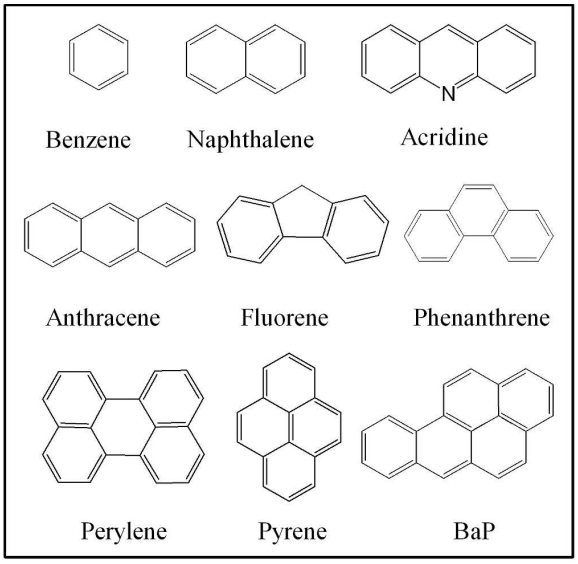
Benzene
Naphthalene
N
Acridine
Anthracene
Fluorene
Phenanthrene
Perylene
Pyrene
BaP

Figure 1.

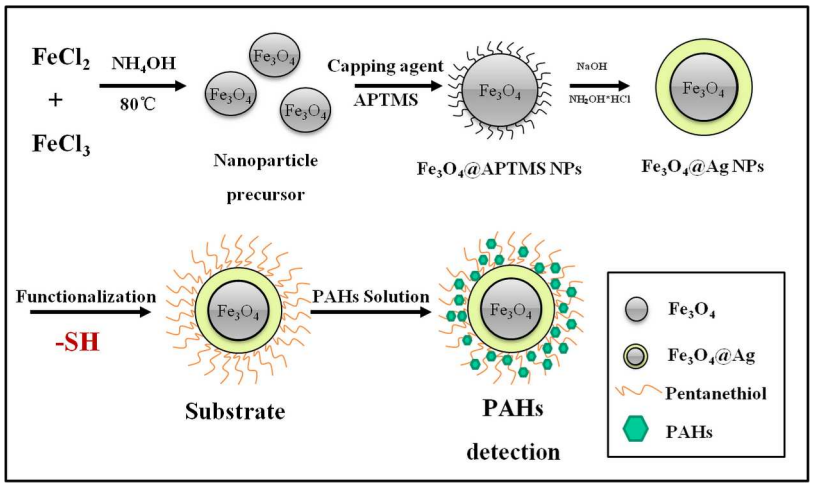
FeCl2
+
FeCl3
NH4OH
80℃
Fe3O4
Fe3O4
Fe3O4
Nanoparticle
precursor
Capping agent
APTMS
Fe3O4
Fe3O4@APTMS NPs
NaOH
NH2OH*HCl
Fe3O4
Fe3O4@Ag NPs
Functionalization
-SH
Fe3O4
Substrate
PAHs Solution
Fe3O4
PAHs
detection
Fe3O4
Fe3O4@Ag
Pentanethiol
PAHs

Figure 2.

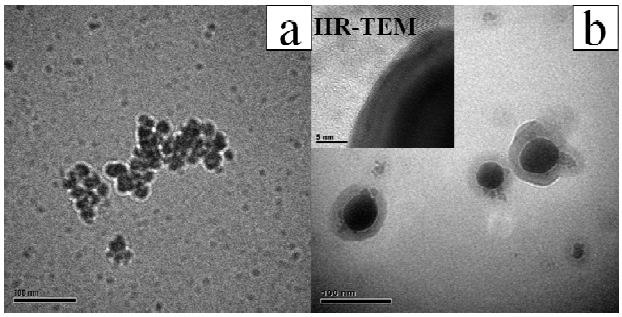

384

385

386

387

388

389

390

391

392

393

394

395

396

397

398 Figure 3.

399

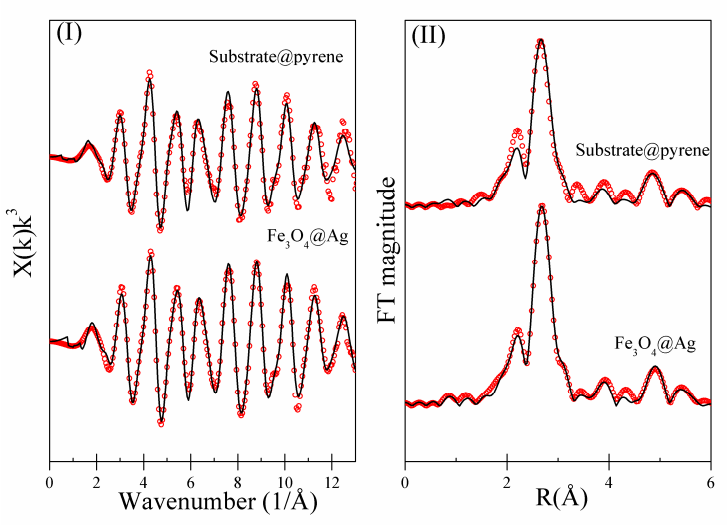
(I)
Substrate@pyrene
Fe3O4@Ag
X(k)k3
Wavenumber (1/Å)
(II)
Substrate@pyrene
Fe3O4@Ag
FT magnitude
R(Å)

Figure 4.

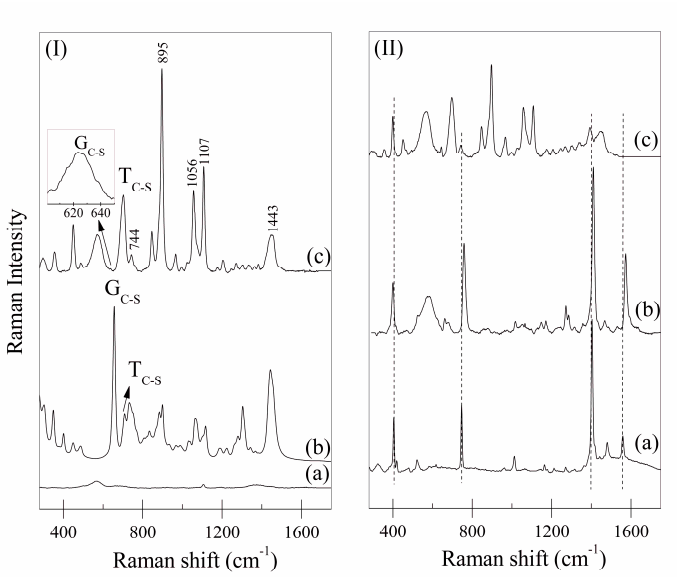

414

415

416

417

418

419

420

421

422

423

424

425 Figure 5.

426

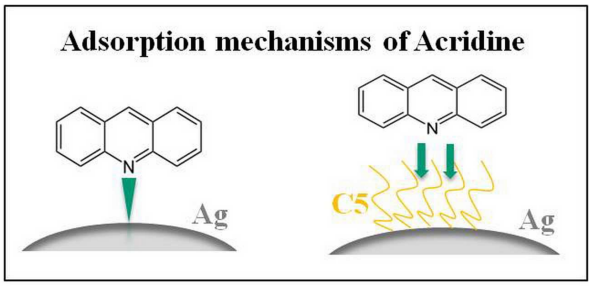

427

428

429

430

431

432

433

434

435

436

437

438

439

440

441 Figure 6

442

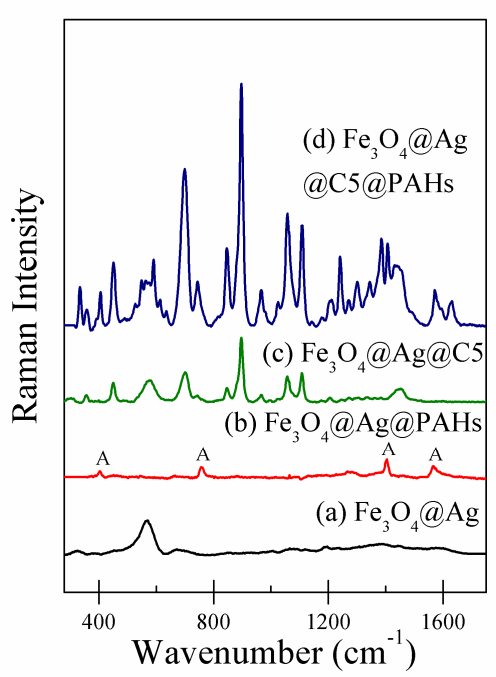

443

444

445

446

447

448

449

450

451

452

453 Figure 7.

454

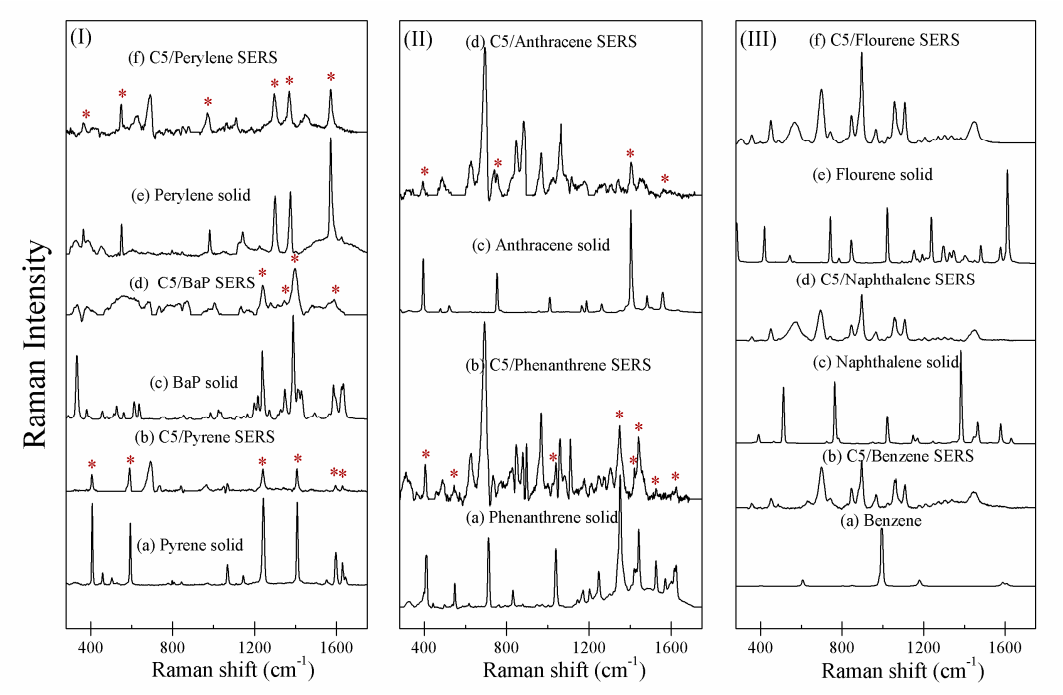

455

456

457

458

459

460

461

462

463

464

465 Figure 8.

466

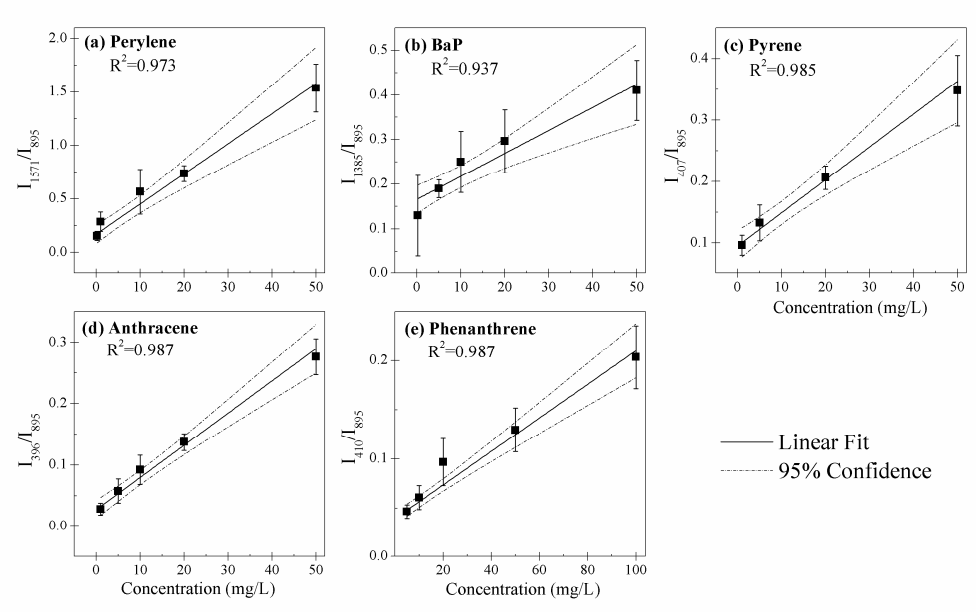
(a) Perylene
R²=0.973
(b) BaP
R²=0.937
(c) Pyrene
R²=0.985
(d) Anthracene
R²=0.987
(e) Phenanthrene
R²=0.987
I1571/I895
I1385/I895
I407/I895
I396/I895
I410/I895
Concentration (mg/L)
Concentration (mg/L)
Concentration (mg/L)
Linear Fit
95% Confidence

Figure 9.

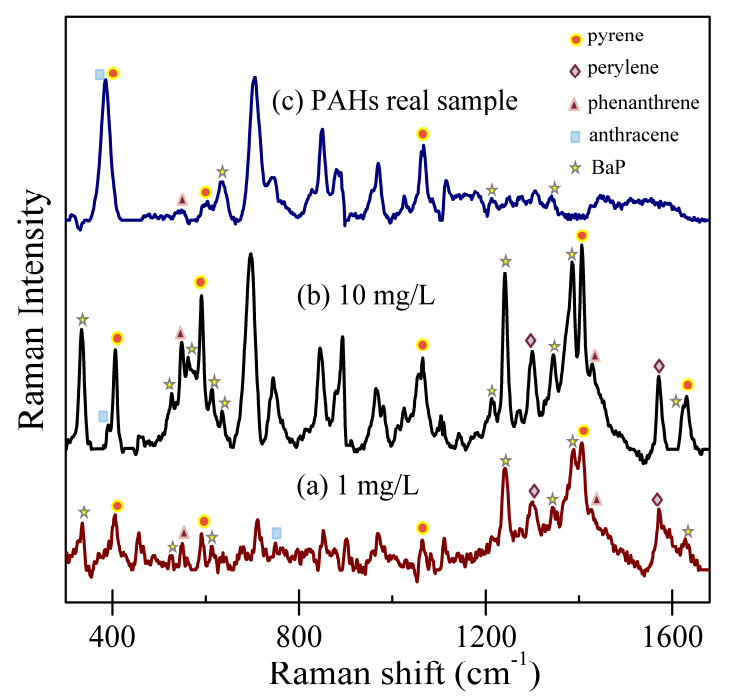

480

481

482

483

484

485

486

487

488

489

490 Figure 10

491

492 TOC Image

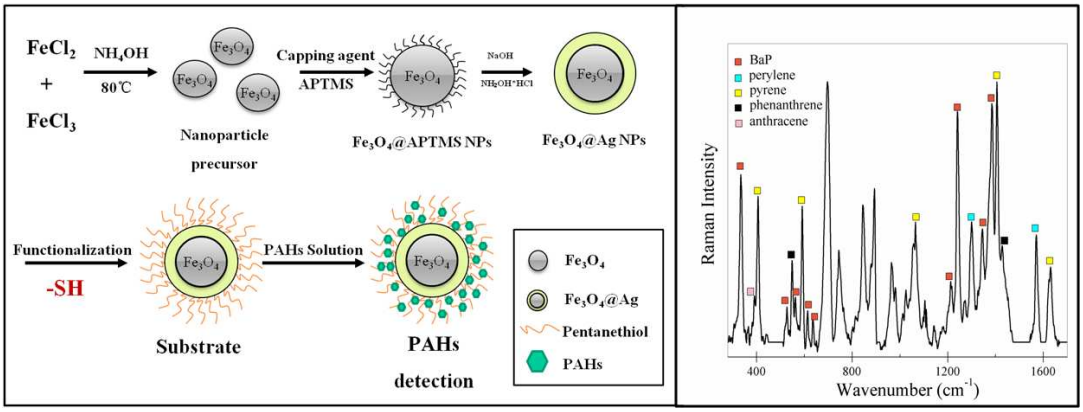

493